Periodic structures with exponentially varying cross-section areas

Camila A. X. da Silva[1], Paulo J. P. Gonçalves[1]

[1]*Dept. of Mechanical Engineering, São Paulo State University (Unesp), College of Engineering, Campus Bauru*
Av. Eng. Luís Edmundo Carrijo Coube, 14-01 – Vargem Limpa, Bauru, 17033-360, São Paulo, Brazil
camila.albertin@unesp.br, paulo.paupitz@unesp.br

Abstract. Periodic structures have been used for many years in different areas such as aerial and terrestrial vehicles, civil engineering structures and many other products. The term periodic structures come from the repetitive arrangements of smaller structural units, also known as cells. Among the different phenomena concerning wave propagation of such systems, the most important is probably the Bragg scattering effect. The Bragg scattering occurs when the wavelength becomes of comparable size to the structural cells. This results in frequency ranges where waves cannot propagate, known as bandgaps. In this context, this paper proposes the study of the formation of bandgaps on a mono-coupled periodic structure consisting of longitudinal wave propagation in rods. The paper proposes the modeling and analysis of finite periodic structures with exponentially varying cross-section area. An investigation is conducted on the effects of using symmetric and asymmetric cell matrices. The structure is modeled using the receptance and dynamic stiffness matrices. The transfer matrix method is used to determine the properties of the structure from the transmissibility of a single cell. Results show that asymmetric cells have a wider frequency range when compared to symmetric cells; however, occurring at higher frequencies ranges.

Keywords: periodic structures, exponentially varying cross-section, bandgap, symmetrical structure, asymmetric structure.

1 Introduction

Periodic structures are arrangements of structural units that have periodicity, where these units are called cells. Recently, the study of periodic structures in mechanical vibrations has been of great interest in the scientific community, mainly because these structures present the phenomenon known as the Bragg scattering effect. This phenomenon occurs when the wavelength becomes comparable to the length of structural cells, resulting in frequency regions where waves do not propagate. Such regions are known as bandgaps [1].

The study of periodic structures probably began with the work by Lord Rayleigh [2] that investigated continuous periodic structures. Later, in the 90's decade, the study regained attention by the pioneering work of Mead [3]. In recent years, several areas of engineering have approached the structural vibration of periodic systems, such as in civil engineering with the use of a new type of periodic foundation to serve as a vibration isolator [4], and for the control of seismic events [5-6]. A novel compounded gearbox periodic strut was used to control noise in a helicopter cabin [7]. Applications, in general, seek to optimize the attenuation bands to reduce vibration propagation within a specific frequency range, usually at lower frequencies.

Recent research shows the behavior of periodic structures of finite and infinite structures [8], and also, in the case of mono-coupled periodic structures composed of symmetric and asymmetric cells [9]. In this context, this paper proposes the study to obtain the so-called bandgaps on a mono-coupled periodic structure consisting of longitudinal wave propagation in rods. The rod is composed of finite periodic structures with exponentially varying cross-sectional areas. The theory of longitudinal wave propagation in rods with variable cross-sections is well developed in the literature [10]. Gan et al. [11] discuss the wave propagation in two examples of non-uniform rods, one of them with the cross-section varying exponentially. The authors developed a study considering the traditional theories of Love and Mindlin-Herrmann [12].

The approach used in this work is based on the attenuation band, specifically, the ones that occur at the lower frequencies ranges. Also, attention is given to the bandwidth of this bandgap and the maximum attenuation frequency within this band.

The structure is modeled using the dynamic stiffness and receptance matrices. The transfer matrix is used to determine structure properties based on the transmissibility of a single cell. The transfer matrix is an alternative formulation that groups the applied forces and the resulting displacement at a given point in a state vector, resulting in reduced computational effort due to mathematical simplicity [13].

2 Modeling of a rod with variable cross-section area

The system shown in Fig. 1(a) is a rod with variable cross-section. The cross-section area changes according to an exponential function. At the left-hand side, the cross-section is defined by $A_0 = \pi r_0^2$. At position x, the cross-section is given by $A(x) = A_0 e^{2\beta x}$. The other rod properties are the Young's Modulus E, mass density ρ and the length l.

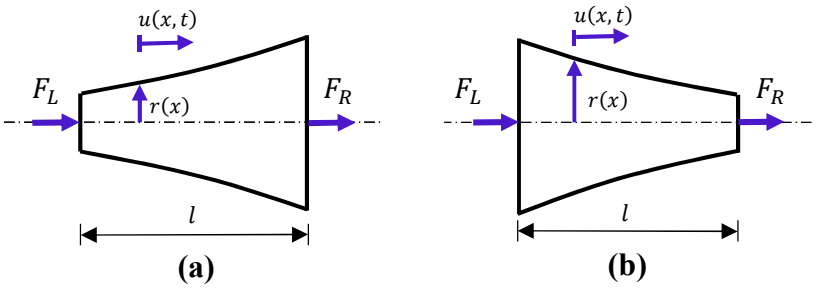

Figure 1: A rod with the cross-sectional area of varying in exponential

According to Graff [10], the differential equation of the motion in the space domain is given by

$$U''(x) + \frac{A'(x)}{A(x)} U'(x) + k_0^2 U(x) = 0 \tag{1}$$

where $k_o = \omega\sqrt{\rho/E}$ is the wave number of a rod with cross-section. With the cross-section governed by equation $A(x) = A_0 e^{2\beta l}$ the equation of motion in space domain reduces to

$$U''(x) + 2\beta U'(x) + k_0^2 U(x) = 0 \tag{2}$$

To obtain the equation that describes the wave dispersion, assume the solution of the form $U(x) = Ue^{-jkx}$ and substitute in equation (2):

$$-k^2 - j2\beta k + k_0^2 = 0\,, \tag{3}$$

equation (3) has two solutions given by

$$k_{1,2} = -j\beta \pm \sqrt{k_0^2 - \beta^2} = -j\beta \pm \hat{k} \tag{4}$$

where $\hat{k} = \sqrt{k_0^2 - \beta^2}$. The real and imaginary parts of the two wavenumbers are shown in Fig. 2, which represent dispersion curves for a rod with exponentially varying cross-section area, where the following properties were considered $E = 3 \times (1 + 0.01j)$ GPa, $\rho = 1130$ Kg/m^3, $\beta = 4$, $l = 0.15$ m and $r_0 = 0.0247$ m.

The cut-off phenomenon visualized in Fig. 2 is one of the most typical characteristics of structures with exponential area variation. The real part of the wavenumber is non-zero in the cut-off region. It is known that no purely imaginary wavenumber can exist in lossy structures [14].

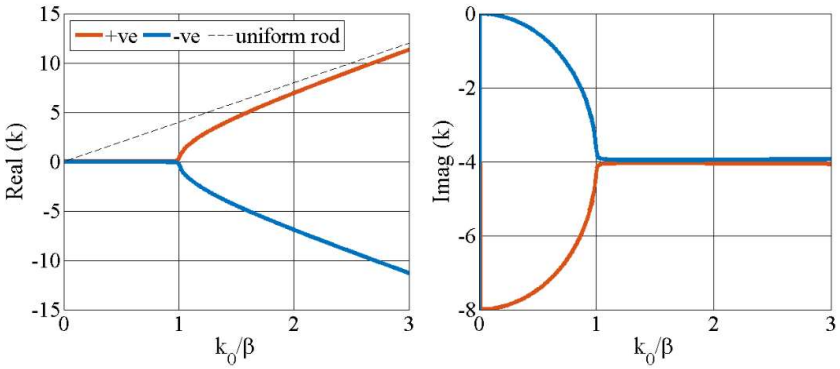

Figure 2: Real and imaginary parts of the wavenumbers with the positive and negative propagating wavenumbers.

To obtain the receptance and dynamic stiffness matrices for a rod with exponentially varying cross-section area assume the following solution $U(x) = c_1 e^{-jk_1 x} + c_2 e^{-jk_2 x}$, where k_1 and k_2 are two wavenumbers and c_1 and c_2 are the associated wave amplitudes. Two boundary conditions are evaluated $EA_0 U'(0) = -F_L|_{F_R=0}$ and $EA_0 e^{2\beta l} U'(l) = F_R|_{F_L=0}$. The receptance and the dynamic stiffness matrices are given by

$$\begin{Bmatrix} U_L^{[A]} \\ U_R^{[A]} \end{Bmatrix} = \frac{\hat{k}}{EA_0 k_0^2} \begin{bmatrix} \frac{\beta}{\hat{k}} - \cot\left(\hat{k}l\right) & -e^{-\beta l}\csc\left(\hat{k}l\right) \\ -e^{-\beta l}\csc\left(\hat{k}l\right) & e^{-2\beta l}\left(-\frac{\beta}{\hat{k}} - \cot\left(\hat{k}l\right)\right) \end{bmatrix} \cdot \begin{Bmatrix} F_L^{[A]} \\ F_R^{[A]} \end{Bmatrix} \tag{5}$$

$$\begin{Bmatrix} F_L^{[A]} \\ F_R^{[A]} \end{Bmatrix} = A_0 E\hat{k} \begin{bmatrix} \frac{\beta}{\hat{k}} + \cot\left(\hat{k}l\right) & -e^{\beta l}\csc\left(\hat{k}l\right) \\ -e^{\beta l}\csc\left(\hat{k}l\right) & e^{2\beta l}\left(-\frac{\beta}{\hat{k}} + \cot\left(\hat{k}l\right)\right) \end{bmatrix} \cdot \begin{Bmatrix} U_L^{[A]} \\ U_R^{[A]} \end{Bmatrix} \tag{6}$$

The system shown in Fig. 1(b) is rod with cross-sectional area of varying exponential decay. As previously considered, the smallest cross-section is defined $A_0 = \pi r_0^2$ which in this configuration is on the right-hand side and the largest cross-section is on the left-hand side, where it is defined by $A_l = A_0 e^{2\beta l}$. At position x, the cross-section is given by $A(x) = A_l e^{-2\beta x}$. The receptance and the dynamic stiffness matrices are given by

$$\begin{Bmatrix} U_L^{[B]} \\ U_R^{[B]} \end{Bmatrix} = \frac{\hat{k}}{EA_0 k_0^2} \begin{bmatrix} e^{-2\beta l}\left(-\frac{\beta}{\hat{k}} - \cot\left(\hat{k}l\right)\right) & -e^{-\beta l}\csc\left(\hat{k}l\right) \\ -e^{-\beta l}\csc\left(\hat{k}l\right) & \frac{\beta}{\hat{k}} - \cot\left(\hat{k}l\right) \end{bmatrix} \cdot \begin{Bmatrix} F_L^{[B]} \\ F_R^{[B]} \end{Bmatrix} \tag{7}$$

$$\begin{Bmatrix} F_L^{[B]} \\ F_R^{[B]} \end{Bmatrix} = A_0 E\hat{k} \begin{bmatrix} e^{2\beta l}\left(-\frac{\beta}{\hat{k}} + \cot\left(\hat{k}l\right)\right) & -e^{\beta l}\csc\left(\hat{k}l\right) \\ -e^{\beta l}\csc\left(\hat{k}l\right) & \frac{\beta}{\hat{k}} + \cot\left(\hat{k}l\right) \end{bmatrix} \cdot \begin{Bmatrix} U_L^{[B]} \\ U_R^{[B]} \end{Bmatrix} \tag{8}$$

3 Transfer matrix of the periodic structure composed of N cells

A mono-coupled periodic structure composed of N identical periodic cells is shown in Fig. 3

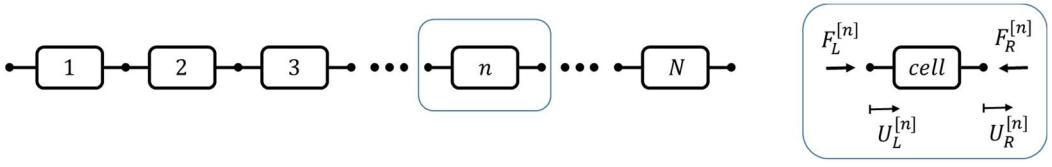

Figure 3: General one-dimensional structure comprised of N periodic cells. Adapted from [15].

The relationship between the force and displacement at the right end of the structure in Fig.3 to the force and displacement at the left end is given by $q_R^{[N]} = T^N q_L^{[1]}$, where $q_R = \{F_R, U_R\}^T$, $q_L = \{F_L, U_L\}^T$ and $T = \begin{bmatrix} T_{11} & T_{12} \\ T_{21} & T_{22} \end{bmatrix}$ is the transfer matrix of a single cell [16].

From the work of Rubin [16] it is possible to obtain the transfer matrix from the transformation of the dynamic stiffness matrix. Considering the dynamic stiffness matrices given by equations (6) and (8) and applying the transformation proposed by Rubin [16], the transfer matrices are

$$\mathbf{T}_A^{rod} = \begin{bmatrix} e^{\beta l}\left(-\dfrac{\beta}{\hat{k}}\sin\left(\hat{k}l\right)+\cos\left(\hat{k}l\right)\right) & \dfrac{EA_o e^{\beta l}\left(\beta^2+\hat{k}^2\right)\sin\left(\hat{k}l\right)}{\hat{k}} \\ \dfrac{-e^{-\beta l}\sin\left(\hat{k}l\right)}{EA_o\hat{k}} & e^{-\beta l}\left(\dfrac{\beta}{\hat{k}}\sin\left(\hat{k}l\right)+\cos\left(\hat{k}l\right)\right) \end{bmatrix} \tag{9}$$

$$\mathbf{T}_B^{rod} = \begin{bmatrix} e^{-\beta l}\left(\dfrac{\beta}{\hat{k}}\sin\left(\hat{k}l\right)+\cos\left(\hat{k}l\right)\right) & \dfrac{EA_o e^{\beta l}\left(\beta^2+\hat{k}^2\right)\sin\left(\hat{k}l\right)}{\hat{k}} \\ \dfrac{-e^{-\beta l}\sin\left(\hat{k}l\right)}{EA_o\hat{k}} & e^{\beta l}\left(-\dfrac{\beta}{\hat{k}}\sin\left(\hat{k}l\right)+\cos\left(\hat{k}l\right)\right) \end{bmatrix} \tag{10}$$

The four cases shown in Fig. 4 involve sets of symmetrical cells Fig. 4(a) and sets of asymmetrical cells Fig. 4(b).

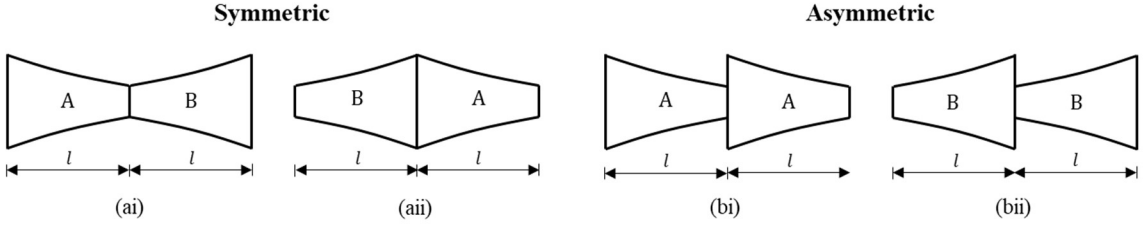

Figure 4: Different configurations of a single cell (ai) and (aii) symmetric cells; (bi) and (bii) asymmetric cells

The transfer matrix for the configurations in Fig. 4 can be obtained from two transfer matrices [9], one for each rod, so that $T^{[Sym]} = T_B^{rod}T_A^{rod}$ for Fig. 4(ai), $T^{[Sym]} = T_A^{rod}T_B^{rod}$ for Fig. 4(aii), $T^{[Sym]} = T_A^{rod}T_A^{rod}$ for Fig. 4(bi) and $T^{[Sym]} = T_B^{rod}T_B^{rod}$ for Fig. 4(bii).

4 Displacement transmissibility of the periodic structure composed of *N* cells

From the transfer matrix, it is possible to obtain the transmissibility $T_r = \left|U_R^{[N]}/U_L^{[1]}\right|$ of a periodic system of N cells. The displacement transmissibility of a symmetric cell system is given by$|1/T_{11}|$ or $|1/T_{22}|$. For asymmetric cells the transmissibility is given by $|1/T_{11}|$ [9]. Thus, the transmissibility of the configurations in Fig. 4 using single-cell are respectively

$$\left|T_r\right|^{[Sym]} = \frac{-\hat{k}^2}{2\left(\hat{k}^2+\beta^2\right)\sin^2\left(\hat{k}l\right)-\hat{k}^2}, \quad \text{for Fig. } 4(ai) \text{ and Fig. } 4(aii) \tag{11}$$

$$\left|T_r\right|^{[Asym]} = \frac{-\hat{k}^2 e^{2\beta l}}{\left(\hat{k}^2+\beta^2\right)e^{2\beta l}\sin^2\left(\hat{k}l\right)-\left(\hat{k}\cos\left(\hat{k}l\right)+\beta\sin\left(\hat{k}l\right)\right)^2}, \quad \text{for Fig } 4(bi) \tag{12}$$

$$\left|T_r\right|^{[Asym]} = \frac{-\hat{k}^2}{\left(\hat{k}^2+\beta^2\right)\sin^2\left(\hat{k}l\right)-e^{2\beta l}\left(\hat{k}\cos\left(\hat{k}l\right)-\beta\sin\left(\hat{k}l\right)\right)^2}, \quad \text{for Fig. } 4(bii) \tag{13}$$

The displacement transmissibility of the cells in Fig. 4 are plotted in Fig. 5, considering the cases of one, and three cells. The transmissibility of the cells in Fig. 4(ai) and Fig. 4(aii), as seen in equation (11), are equal. Bandgap limits and the minimum of transmissibility within the frequency band are also plotted.

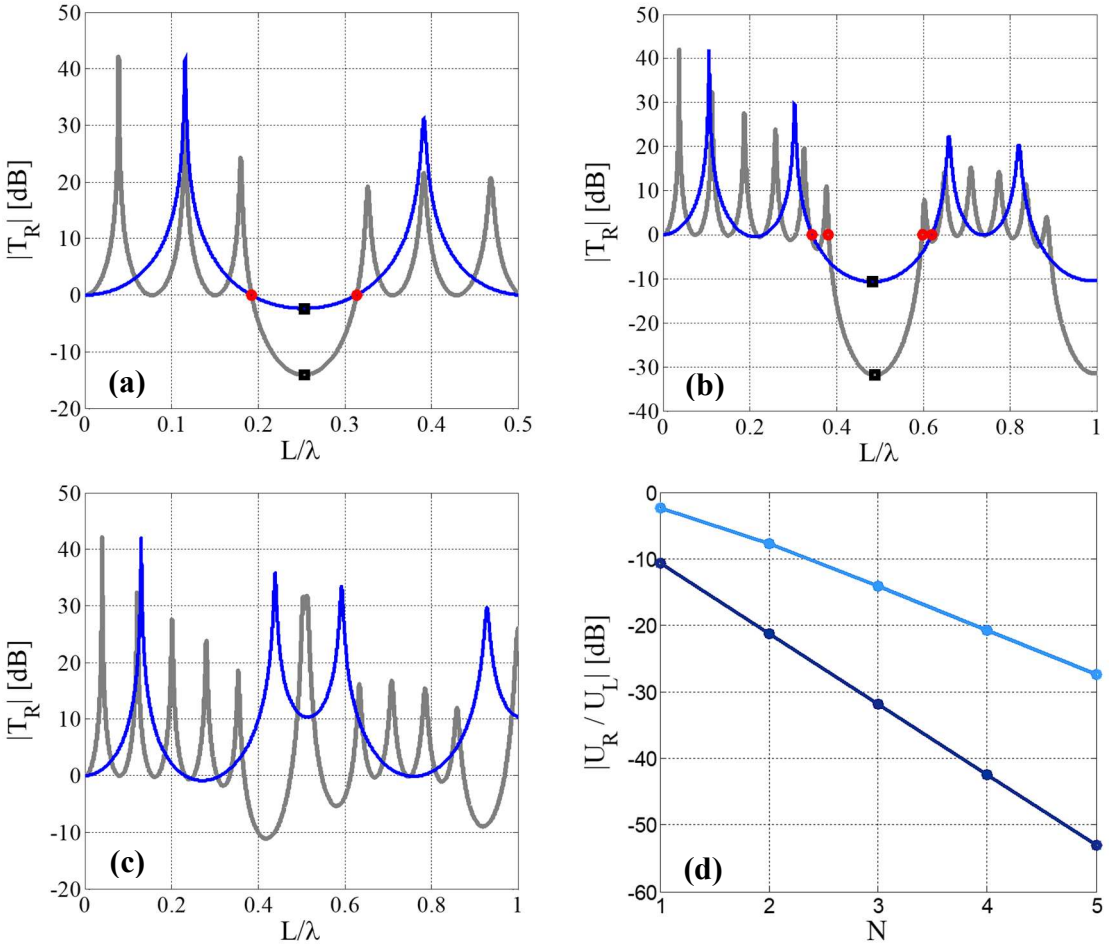

Figure 5: Displacement transmissibility of a periodic structure with (a) symmetric cells; (b) asymmetric cells Fig. 4(bi); (c) asymmetric cells Fig. 4(bii); blue line $N = 1$ cell; gray line $N = 3$ cells; the red circles provide the stop-band limits and the black square gives the maximum attenuation frequency within frequency band; (d) minimum of transmissibility within frequency band in relation to the number of cells; light blue line = symmetric cell; dark blue line = asymmetric cell.

The displacement transmissibility response of a structure composed of symmetrical cells is represented in Fig. 5(a). Note in the figure that the increase in the number of cells does not interfere with the lower and upper limits of the stop-band, which continue with the same values from $\frac{L}{\lambda_{lower}} = 0.1929$ to $\frac{L}{\lambda_{upper}} = 0.2140$. The maximum attenuation, represented by the black squares in Fig. 5(a), has a linear increase as the number of cells increases. This linear increase can be seen in Fig. 5(d) through the light blue line.

Figures 5(b) and 5(c) show the responses of the transmissibility of displacement of a structure composed of asymmetric cells. Note that Fig. 5(b) presents a wider stop-band when compared to the stopping band obtained by structure of symmetrical cell, with values of $\frac{L}{\lambda_{lower}} = 0.3450$ to $\frac{L}{\lambda_{upper}} = 0.6203$ for single cell, however note that that frequency band is in a higher frequencies range. Consequently, the maximum attenuation is also at a higher frequency. Still, in Fig. 5(b) it is possible to observe that the stop-band decreases as the number of cells increases. The maximum attenuation, represented by the black squares in Fig. 5(b), it also presents a linear increase as the number of cells increases. This linear increase can be seen in Fig. 5(d) through the dark blue line.

Fig. 5(c) does not present the stop-band, which highlights the importance of the orientation of the asymmetric structure in relation to the position of the excitation force. Thus, for the asymmetric cell structure to present the attenuation band, it is necessary to orient the thinner side of the structure alongside the excitation force.

The displacement transmissibilities of structures composed of symmetrical cells Fig. 4(ai) and Fig. 4(bi) or asymmetrical Fig. 4(bii) are analyzed in relation to the values of β. For this, the graphs shown in Fig. 6 are plotted,

in which the lower and upper limits of the stop-band and the maximum attenuation are also plotted.

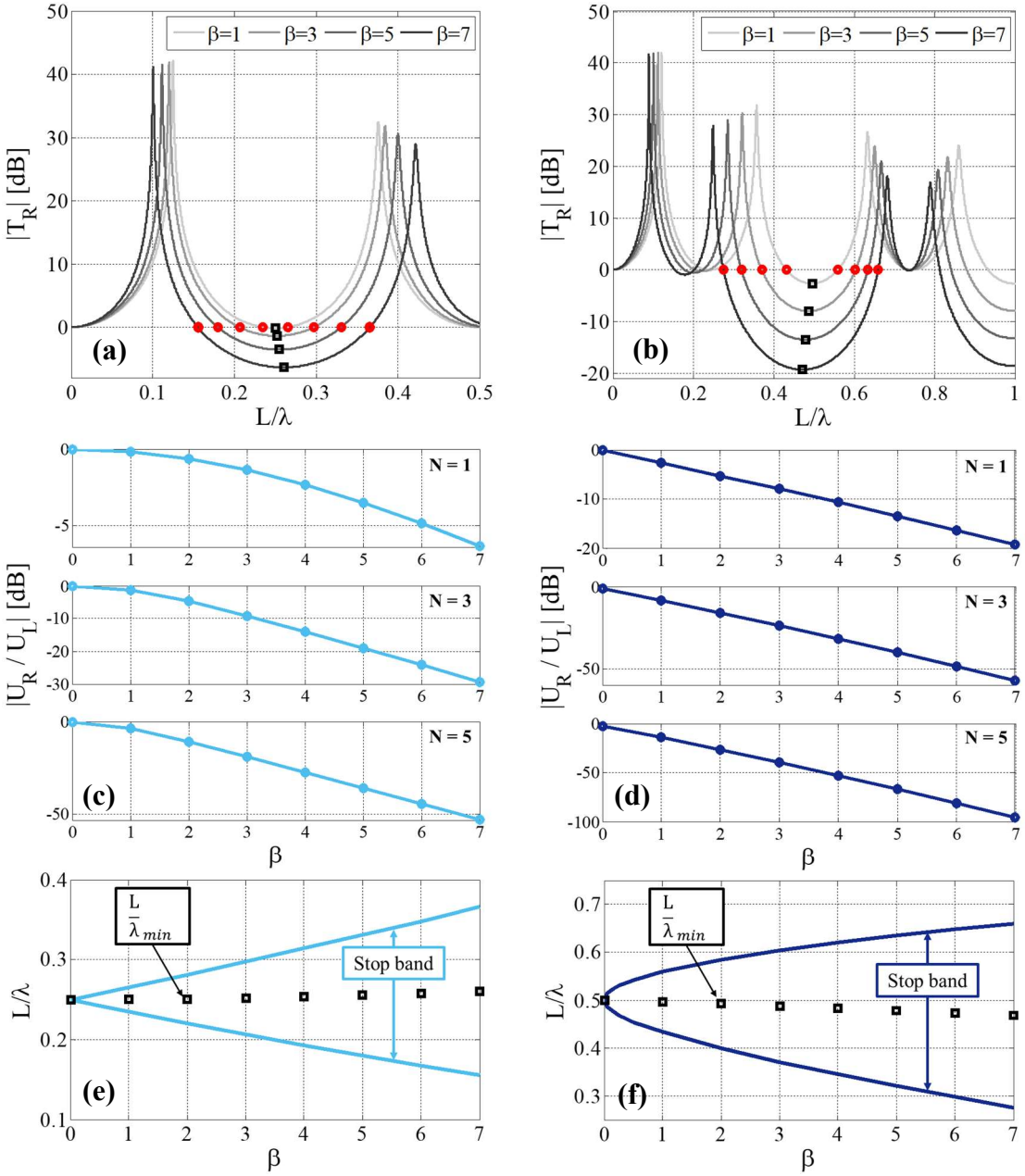

Figure 6: Displacement transmissibility of a periodic structure with different β values (a) symmetric cells; (b) asymmetric cells Fig. 4(bi); the red circles provide the stop band limits and the black square gives the maximum attenuation frequency within frequency band; (c) and (d) Minimum transmissibility in relation to the β values; light blue line = symmetric cell; dark blue line = asymmetric cell; (e) and (f) Stop band as a function of the β; light blue line = symmetric cell; dark blue line = single asymmetric cell .

Figures 6(a) and 6(b) show the responses of the transmissibility of displacement of structures composed of symmetrical or asymmetrical cells, with β values equal to one, three, five and seven. Note that in both cases, as β increases, the maximum attenuation and the stop-band increase. Such behavior can also be seen by Fig. 6(c) and 6(e) for symmetric cells and by Fig. 6(e) and 6(f) for asymmetric cells. It is also possible to observe in the case of symmetric cells, that the maximum attenuation, represented by the black squares in Fig. 6(a), has a small displacement to the higher frequencies. As for the stop band, this one presents a higher magnification on the right side than on the left side.

In the case of asymmetric cells, the maximum attenuation, represented by the black squares in Fig. 6(b), has a small displacement to the lower frequencies. As for the stop-band, this one presents a higher magnification on the left side than on the right side.

5 Conclusions

This paper investigated the propagation of longitudinal waves in a rod composed of N cells, with exponentially varying cross-section area. First, it investigated the behavior of the structure when composed of symmetrical or asymmetrical cells. From this investigation, it was verified the importance of the orientation of the asymmetric cells in relation to the excitation force, in which to obtain the attenuation band, the thinner side of the rod must be oriented next to the excitation force. Furthermore, asymmetric cells when correctly oriented present a wider attenuation band when compared to symmetric cells, however in higher frequency ranges. Regarding the number of cells, the attenuation band of asymmetric cells reduces as the number of cells increases, while in the case of symmetric cells the attenuation band remains the same, only increasing the maximum attenuation within the band.

Subsequently, the behavior of the frequency band and the maximum attenuation in relation to the β value in structures with symmetrical or asymmetrical cells was investigated. In both cases, the higher the β value, the higher the band of attenuation and maximum attenuation. However, in the case of symmetrical cells, the maximum attenuation occurs at higher frequencies as β increases and in the case of asymmetric cells, the opposite occurs, the maximum attenuation occurs at lower frequencies as β increases.

Thus, in view of the proposed study, it was found that periodic structures composed of correctly oriented symmetrical or asymmetrical cells are valid for vibration attenuation and present vibration attenuation in frequency bands distinct from each other.

Acknowledgements. The authors would like to acknowledge the financial support of the São Paulo Research Foundation (FAPESP) Grant Number 2018/15894-0, São Paulo State University (UNESP), and Coordination for the Improvement of Higher Education Personnel (CAPES).

Authorship statement. The authors hereby confirm that they are the sole liable persons responsible for the authorship of this work, and that all material that has been herein included as part of the present paper is either the property (and authorship) of the authors, or has the permission of the owners to be included here.

References

[1] J. M. Mencik, V. Denis, M. Caliez, S. Méo, "Application of the wave finite element method to the analysis of locally resonant band gaps in periodic structures with viscoelastic properties". Conference: ISMA 2018, 2018.
[2] J. W. S. Rayleigh, "The theory of Sound", vol. 1, Dover, New York, 1945.
[3] D. J. Mead, "Wave propagation in continuous periodic structures: Research contributions from Southampton, 1964-1995", *Journal of Sound and Vibration*, vol. 190, pp. 495–524, 1996.
[4] H. J. Xiang, Z. F. Shi, S. J. Wang. Y. L. Mo, "Periodic materials-based vibration attenuation in layered foundations: experimental validation". *Smart Materials and Structures*, vol. 21, n. 11, 2012.
[5] Z. B. Cheng, Z. F. Shi, "Composite periodic foundation and its application for seismic isolation*". Earthquake Engineering & Structural Dynamics*, vol. 47, pp. 925–944, 2017.
[6] Z. Cheng, Z. Shi, A. Palermo, H. Xiang, W. Guo, A. Marzani, "Seismic vibrations attenuation via damped layered periodic foundations". *Engineering Structures*, vol. 211, 2020.
[7] J. T. Szefi, E. C. Smith, G. A. Lesieutre, "Design And Testing Of A Compact Layered Isolator For High frequency Helicopter Gearbox Isolation", *Structural Dynamics & Materials Conference*, pp. 1-13, 2004.
[8] P.G. Domadiya, E. Manconi, M. Vanali, L. V. Andersen, A. Ricci, "Numerical and experimental investigation of stop bands in finite and infinite periodic one-dimensional structures", *Journal of Vibration and* Control, vol. 22 pp. 920–931, 2016.
[9] J. P. Carneiro Jr., M. J. Brennan, P. J. P. Gonçalves, V. G. Cleante, D. D. Bueno, R. B. Santos, "On the Attenuation of Vibration using a Finite Periodic Array of Rods Comprised of Either Symmetrical or Asymmetrical Cells". *J. Sound Vib.*, 2021.
[10] K. F. Graff, "Wave motion in elastic solids", Dover Publications, 1991.
[11] C. Gan, Y. Wei, S. Yang, "Longitudinal wave propagation in a rod with variable cross-section". *J. Sound Vib*, 2014.
[12] M. Krawczuk, J. Grabowska, M. Palacz, "Longitudinal wave propagation. Part I-Comparison of rod theories ". *Journal of Sound and Vibration,* vol. 295, pp. 461-478, 2006.
[13] P. Gardonio, M.J. Brennan, "Mobility and impedance methods in structural dynamics". In: F. Fahy, J. Walker (eds.), *Advanced Applications in Acoustics, Noise and Vibration*, 1st ed., Spon Press, London, pp. 389–447, 2004.
[14] M. K. Kalkowski, J. M. Muggleton, E. Rustighi, "Wave propagation in rods with an exponentially varying cross-section - Modelling and experiments". *Journal of Physics: Conference Series*, vol. 744, pp. 1-12, 2016.
[15] P. J. P. Gonçalves, M. J. Brennan, V. G. Cleante, "Predicting the stop-band behavior of finite mono-coupled periodic structures from the transmissibility of a single element". *Mechanical Systems and Signal Processing,* vol. 154, pp. 1-17, 2021.
[16] S. Rubin, "Mechanical Immittance-and Transmission-Matrix Concepts". *The Journal of the Acoustical Society of America,* vol. 41, n. 5, pp. 1171–1179, 1967.